ADVANCED FUNCTIONAL MATERIALS
www.afm-journal.de

Demystifying the Semiconductor-to-Metal Transition in Amorphous Vanadium Pentoxide: The Role of Substrate/Thin Film Interfaces

A. Carmel Mary Esther, G. Mohan Muralikrishna, Manohar Chirumamilla, Manoel da Silva Pinto, Stefan Ostendorp, Martin Peterlechner, Alexander Yu Petrov, Manfred Eich, Sergiy V. Divinski, Horst Hahn, and Gerhard Wilde*

The precise mechanism governing the reversible semiconductor-to-metal transition (SMT) in V_2O_5 remains elusive, yet its investigation is of paramount importance due to the remarkable potential of V_2O_5 as a versatile "smart" material in advancing optoelectronics, plasmonics, and photonics. In this study, distinctive experimental insights into the SMT occurring in amorphous V_2O_5 through the application of highly sensitive, temperature-dependent, in situ analyses on a V_2O_5 thin film deposited on soda-lime glass are presented. The ellipsometry measurements reveal that the complete SMT occurs at ≈340 °C. Remarkably, the refractive index and extinction coefficients exhibit reversible characteristics across visible and near-infrared wavelengths, underscoring the switch-like behavior inherent to V_2O_5. The findings obtained from ellipsometry are substantiated by calorimetry and in situ secondary ion mass spectrometry analyses. In situ electron microscopy observations unveil a separation of oxidation states within V_2O_5 at 320 °C, despite the thin film retaining its amorphous state. The comprehensive experimental investigations effectively demonstrate that alterations in electronic state can trigger the SMT in amorphous V_2O_5. It is revealed for the first time that the SMT in V_2O_5 is solely contingent upon electronic state changes, independent of structural transitions, and importantly, it is a reversible transformation within the amorphous state itself.

1. Introduction

In 1954, Denton et al. published the first report on the vitrification of vanadium pentoxide (V_2O_5).[1,2] This early publication indirectly indicated that the range of linear thermal expansion of V_2O_5-based glass is limited to 250 °C. Further, Aldebert et al.[3] reported differential thermal analysis and thermogravimetry data of V_2O_5 gel with a prominent endothermic peak at ≈300 °C and an exothermic peak ≈350 °C. Since the weight loss at 300 °C was very weak, the authors related the endo- and exo-thermic peaks to the dissociation of a strongly bonded minor fraction of H_2O. Further, the report clearly mentioned that the major portion of H_2O dissociated at temperatures below 270 °C. Additionally, the observed process was reversible and involved a significant modification of the coordination of V^{4+}. Later reports for V_2O_5 thin films indicated the occurrence of a metal-to-insulator transition (MIT) at three different temperatures of ≈127,[4] 260,[5] and 338 °C.[6]

A. C. M. Esther, G. M. Muralikrishna, M. da S. Pinto, S. Ostendorp, M. Peterlechner, S. V. Divinski, G. Wilde
Institute of Materials Physics
University of Münster
48149 Münster, Germany
E-mail: garlapat@uni-muenster.de

G. M. Muralikrishna, H. Hahn
Institute for Nanotechnology (INT)
Karlsruhe Institute of Technology
Kaiserstraße 12, 76131 Karlsruhe, Germany

M. Chirumamilla, A. Yu Petrov, M. Eich
Institute of Optical and Electronic Materials
Hamburg University of Technology
Eissendorfer Strasse 38, 21073 Hamburg, Germany

M. Chirumamilla
Aalborg University
Skjernvej 4A, Aalborg Øst 9220, Denmark

A. Yu Petrov, M. Eich
Helmholtz-Zentrum Hereon
Max-Planck-Strasse 1, 21502 Geesthacht, Germany

H. Hahn
School of Sustainable Chemical
Biological and Materials Engineering
The University of Oklahoma
100 E. Boyd St., Norman, OK 73019, USA

The ORCID identification number(s) for the author(s) of this article can be found under https://doi.org/10.1002/adfm.202309544

DOI: 10.1002/adfm.202309544

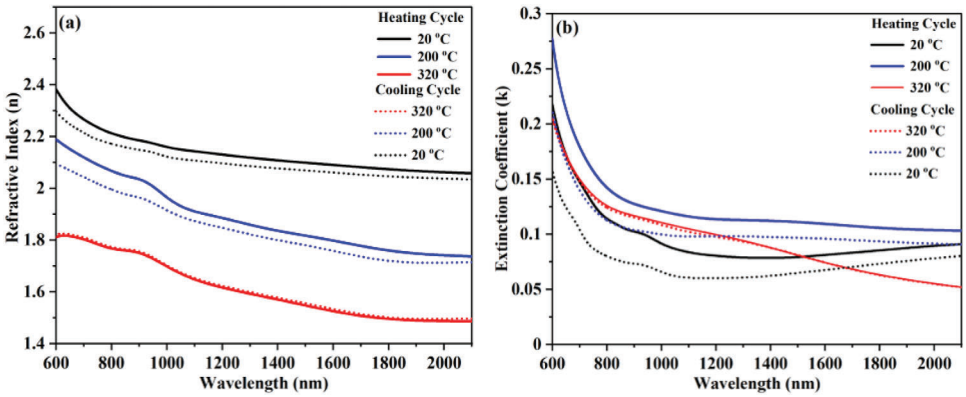

Figure 1. Optical constants as a function of temperature in the spectral region of 600–2100 nm: a) refractive index and b) extinction coefficient.

Blum et al.[4] proposed a defect-induced reversible MIT for surfaces of single-crystalline V_2O_5. It was argued that, since this was supposedly only a surface phenomenon, it should thus predominantly occur in ultrathin films. However, the report did not conclude the conditions responsible for the reversibility.[4] Later, Kang et al.[5] suggested the occurrence of a reversible "non-structural" phase transition. Naturally, this suggestion triggered controversies[7] as the phenomenon of a phase transition often implies the occurrence of a structural change. Porwal et al.[6] reported a reversible phase transition of amorphous V_2O_5 at a transition temperature between ≈335 and 340 °C while the transition temperature was independent of the film thickness over the range of ≈25 to 240 nm.[6] On the other hand, a phase transition temperature < 90 °C was reported for VO_2 and also for other vanadium oxide-based systems in the presence of a second metallic phase viz. composite structures[8] with a metallic dispersion,[9,10] coated on metal substrates,[11] vanadium oxide/metal multilayers[12] or nanostructures.[13,14] However, the transition temperature values reported in the aforementioned studies are rather scattered and no systematics can be deduced. For example, a V_2O_5-MoO_x composite system shows a transition temperature of ≈45 °C[9] but co-doping by F with Mo and Ti induced a transition temperature of ≈−24 to −26 °C.[15] In conclusion, for both metal-doped VO_2[16–18] and V_2O_5[9] systems, a reduction of the MIT down to near room temperature and even sub-zero Celsius temperatures was reported. V_2O_5 exhibits semiconductor behavior and theoretically is expected to attain metallic behavior above the transition temperature, thus the transition in V_2O_5 is referred to as Semiconductor-to-Metal Transition (SMT) in the current study.

The SMT in vanadium oxide still remains unresolved and at the same time it offers fascinating opportunities for applications in advanced optoelectronics and photonics.[19] From a wider perspective, the studies on the conductivity change in vanadium oxides are often correlated with the variation in structural,[14,20–22] magnetic,[23,24] strain-induced[14,25,26] or defect induced[4] effects. Recently, for the first time, an interfacial reaction-induced SMT was reported in amorphous vanadium pentoxide deposited on soda-lime glass.[27]

V_2O_5 is the basic building block for many functional applications[28–31] therefore, in-depth analyses to trace the origin of the SMT as a function of temperature are essential. However, the existing literature reports the occurrence of SMT at different temperatures. Despite the diversity in thickness[32] and substrates investigated, there remains a lack of clear explanation or direct correlation[4,6–9,11–18] which demands the examination of factors influencing the SMT in V_2O_5. This includes understanding the SMT in different forms of vanadium oxide, such as crystalline, multilayered, doped, and composite materials.[19] Each of these aspects requires a separate systematic investigation. This underscores the necessity to uncover a fundamental and dependable mechanism for the occurrence of the SMT in V_2O_5. Hence, the current study aims to provide a systematic investigation of the SMT in V_2O_5.

The present work is based on dedicated in situ temperature-based characterizations of amorphous V_2O_5 thin films. In situ ellipsometry is used to investigate the temperature-dependent optical constants of the thin films. In situ, temperature-based electron energy loss spectroscopy (EELS) and electron diffraction within a transmission electron microscope (TEM) were employed to characterize the oxidation state and the amorphous structure of V_2O_5 in the SMT temperature range. Differences in the onset – and peak positions of the V-L_3, V-L_2, and O-K edges of the V_2O_5 were obtained from EELS as a function of temperature. The comprehensive results of the complementing in situ analyses are discussed in detail with respect to the nature of the SMT of V_2O_5.

2. Results and Discussion

Figure 1a,b shows the extracted real (n) and imaginary (k) parts of the complex refractive indices as a function of the wavelength at selected temperatures obtained for an 80 nm V_2O_5 thin film sputtered on a glass substrate. A significant decrement in "n" across the wavelength range is observed when the temperature increases from 20 to 340 °C, whereas a non-monotonous and wavelength-dependent change of the extinction coefficient is observed (in Figure 1b). An increment in "k" is observed when the temperature is raised from 20 to 200 °C, which might be attributed to a higher optical loss of the material at intermediate temperature (of SMT region) in the first heating cycle. Above 200 °C, a decrement in "k" is seen for the high temperature V_2O_5 structure. These "n" and "k" values during the heating and cooling ramps follow the same trends throughout the spectral region. A residual decrease of the extinction coefficient after the

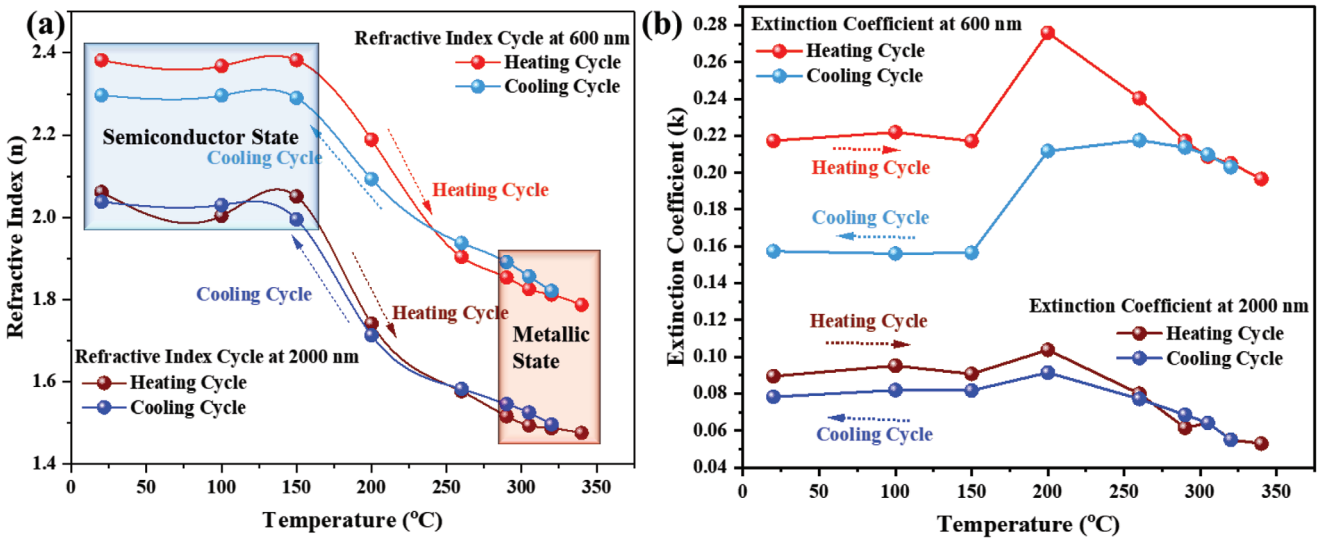

Figure 2. a) Refractive index and b) extinction coefficient, at wavelengths of 600 and 2000 nm, as functions of temperature.

thermal cycle is observed. A high transmissivity and low reflectivity are observed at room temperature throughout the visible to near-infrared spectral region as shown in Figure S1 (Supporting Information) of the supplementary material. The optical constants were further validated by conducting measurements at room temperature and various incidence angles (50°, 60° and 70°), and the results demonstrated consistent behavior irrespective of the angle of incidence (Figure S2, Supporting Information).

Figure 2a,b shows the variation in optical constants "n" and "k", respectively, as a function of temperature at the wavelengths of 600 and 2000 nm, respectively. A decrement in the refractive index is noticed as temperature rises, which then reverts to its initial state upon cooling. An excellent contrast of "n" and "k" is observed for semiconducting and metallic states of the V_2O_5 structure. The SMT is observed to be reversible, as indicated by the similar path of "n" during heating and cooling, with the occurrence of only a minor hysteresis, which is more prominent at a wavelength of 600 nm. Upon heating above 300 °C, the variation of "n" is observed to be minimal/negligible in the temperature range of 300–340 °C and the completeness of the SMT can be assumed. The values of "n" and "k" are found to be in good agreement with the available literature at room temperature.[33–36] However, Kang et al.[5] reported an increase in the n(T) and k(T) values of crystalline V_2O_5 with increasing temperature, in contrast to the findings in our current analysis. This discrepancy could be linked to the defects[37] present in the polycrystalline film resulting from its lossy metallic state, as well as the inhomogeneous structural phases caused by the incorporation of other phases like V_6O_{13} and V_2O_3. At the same time, the trend observed in the current study (Figure 2a,b) closely matches with a report[38] on crystalline VO_2, where a reduction of "n" and a slight increment of "k" at the transition temperature was measured in the wavelength region of visible light.

Figure S3 (Supporting Information) depicts the relative dielectric functions (ε_1 and ε_2) of a V_2O_5 thin film with respect to temperature at a wavelength of 2000 nm. The complex dielectric function $\varepsilon = \varepsilon_1 + i\,\varepsilon_2$ provides the optical properties of the materials and describes material electric polarization and absorption, where ε_1 and ε_2 are the real and imaginary parts of ε, with $\varepsilon_1 = n^2 - k^2$, $\varepsilon_2 = 2nk$.

ε_1 and ε_2 decrease as temperature increases. This change is predominant at 200 °C, while the values of the dielectric functions did not follow the same course during cooling. These effects can be directly correlated to the SMT in V_2O_5, which is discussed in detail in the following sections.

Figure 3 shows the variation in resistivity of the V_2O_5/glass system during repeated heating and cooling cycles. In the given temperature interval, the resistivity of the V_2O_5/glass system (the AC resistivity was averaged for the frequency range of 5 Hz to 1 kHz) varies almost linearly with the temperature between 10^8 to 10^6 ohm cm^{-1}, i.e., within two orders of magnitude (Figure 3).

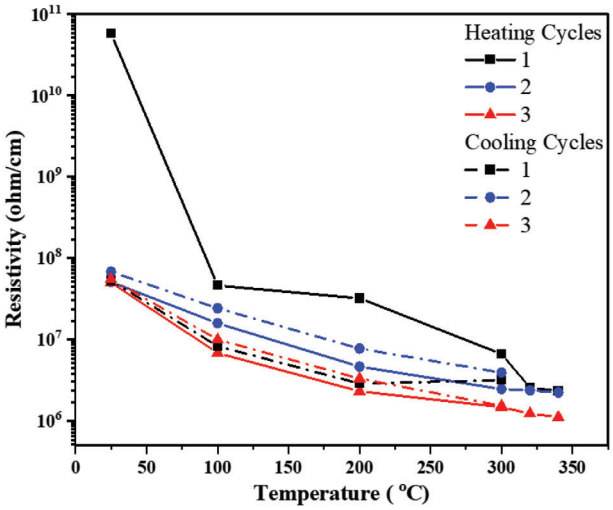

Figure 3. Resistivity during heating and cooling cycles of V_2O_5 thin film deposited on soda-lime glass.

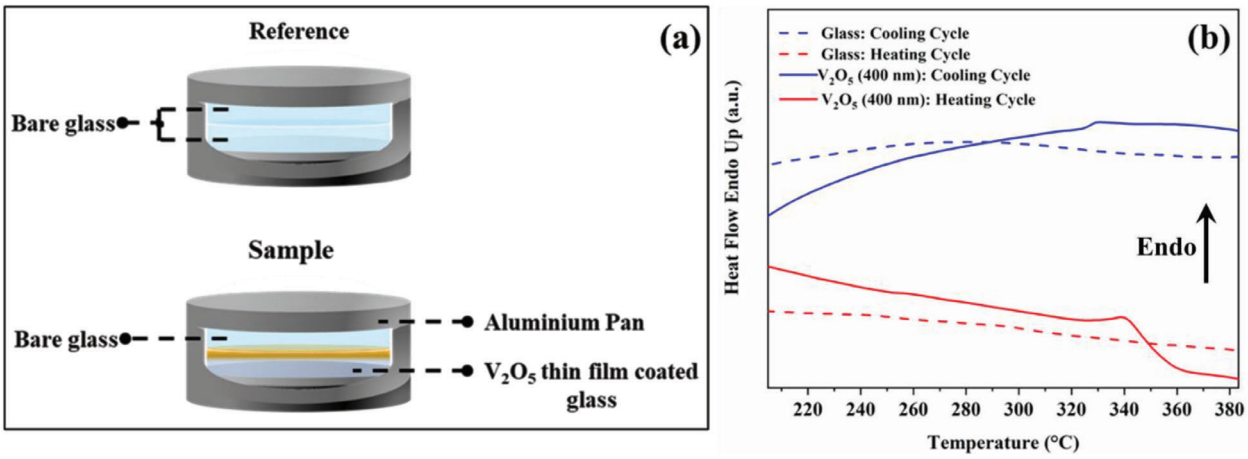

Figure 4. a) Optimized reference and thin film sample configuration for DSC experiments and b) Calorimetric thermogram of the bare glass reference (dashed lines) and with the film-coated (400 nm) on glass (solid lines). The scanning rate was 100 °C min^{-1}.

The heating-cooling hysteresis was found to be minimal for the second and third cycles, after an initial stabilization during the first cycle. The stabilization during the first cycle includes evaporation of adsorbed surface adatoms/molecules.

The heat flow response obtained from the DSC results further supports the SMT in V_2O_5. The procedure followed for the preparation of thin film samples for DSC measurements is shown in **Figure** 4a. Heating and cooling cycles were performed from 20 to 400 °C at 100 °C min^{-1} under high purity Ar atmosphere (1.5 bar). The thin film coating is sandwiched between two tiny glass plates, while the reference sample consists of the bottom and top glass plates alone without the thin film. For reliable heat flow curves, a measurement on the reference sample is necessary and it is used to exclude the influence of the glass substrate. Following this procedure, one can avoid the possible chemical reactions of V_2O_5 with the sample holders (Al, Pt). To increase the signal above the noise level, 400 nm thick V_2O_5 films were used for the DSC measurements. The 400 nm thick V_2O_5 films were deposited by increasing the sputtering time to 5 h and all other deposition parameters were left unchanged. It is to be noted that the SMT in V_2O_5 is independent of the film thickness.[6]

The heat flow curves in the expected reaction region of 190–390 °C that was obtained from the DSC measurements are shown in Figure 4b. V_2O_5 (400 nm)/ glass shows a reaction upon heating, where an endothermic change of the heat flow is noticed. The peak of the transition appeared at 339 °C with the onset and offset temperatures at ≈325 and 360 °C, respectively. Similarly, during cooling, the onset, peak, and offset temperatures were observed at ≈340, 330, and 324 °C, respectively. By comparing the calorimetric signatures observed on the V_2O_5 (400 nm)/ glass system with those from the bare glass substrates, the change in the heat flow after 320 °C can be attributed to the V_2O_5 thin film.

The structural characterization of the as-deposited and heat treated (350 °C, 2 h) thin film samples by X-ray diffraction are presented in Figure S6 (Supporting Information) of the supplementary material depicting the amorphous state of V_2O_5. In-depth analysis of the prepared samples is conducted by TEM and corresponding TEM micrographs of V_2O_5 are shown in Figure S4 (Supporting Information). An on-purpose defocused TEM micrograph (Figure S4b, Supporting Information) resolved nanocluster-like structures of the directly sputter-deposited V_2O_5. The microstructure of the sputter-deposited film is uniform, with a feature size of <90 nm. Furthermore, the purposely under-focused image was utilized to increase the contrast of the thickness variations and it shows that the film that was deposited on the C-coated Cu grid was highly dense and intact. The processing conditions for all three films per substrate combination: V_2O_5 thin film on glass, on C-coated copper grid, and on a TEM proto-chip sample holder were kept similar for the ellipsometry measurements and for the TEM investigation.

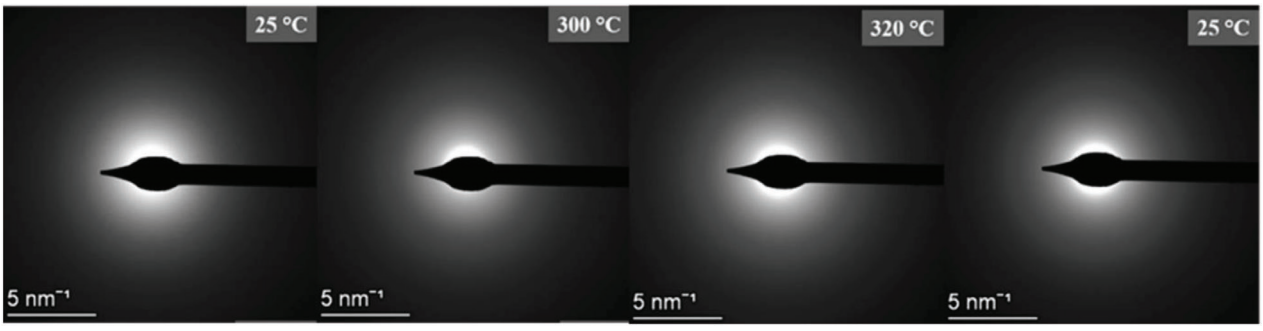

Figure 5. In situ electron beam diffraction patterns acquired during heating and cooling, depict the presence of stable and amorphous V_2O_5 in the whole temperature range of the present study.

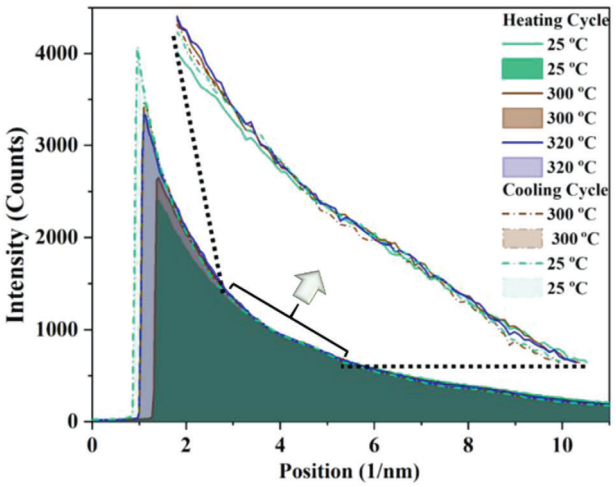

Figure 6. Intensity profiles of the SAED pattern as a function of temperature for both heating and cooling cycles depicting no observable difference in the intensity revealing the stable and amorphous nature of the V_2O_5 thin film in the investigated temperature window.

Figure 5 depicts the selected area electron diffraction (SAED) patterns at selected temperatures. The diffraction patterns show the appearance of a diffuse ring, which is characteristic of the amorphous V_2O_5 structure.[39] The ring is observed to appear during heating to temperatures above ≈270 °C. The intensity profiles of the SAED patterns at selected temperatures are shown in **Figure 6**, which substantiates that the amorphous nature of the deposited vanadium oxide film is stable throughout the entire heating and cooling cycles and the intensity of the diffuse ring is weak. Hence, an in-depth analysis of the recorded series of diffraction patterns (Figures 5 and 6) revealed no structural transformations or nanocrystal formation during the heating and cooling cycles. As the atomic structure of amorphous systems is a complex and still unsolved issue, involving distributions of atomic neighborhoods that are currently described as short- and medium-range order, small structural modifications of the amorphous phase in terms of local rearrangements cannot be excluded. Yet, the occurrence of "disruptive" structural transitions, e.g., the formation of (nano) crystals, can safely be excluded on the basis of our detailed structural analyses.

In situ, temperature-based EELS data of the V-$L_{2,3}$ and O-K edges of amorphous V_2O_5 obtained during heating and cooling cycles are shown in **Figure 7**a,b. An expanded view of the V-$L_{2,3}$ and O-K edges is shown in Figure 7c,d. The oxidization state of amorphous V_2O_5 is determined as V^{5+} from the chemical shifts of the V-L_3 edge in particular from V^{0+} at 513 eV to V^{5+} at 515.2 eV. Within the experimental accuracy (<1 eV) the values agree with the reported values of the V-L_3 edge of single-crystalline V_2O_5 at 515.8 eV, determined by EELS with a dispersion of 0.22 eV.[40] **Table 1** depicts the energy difference of the V-L_3 edge with respect to the V-L_3 edge of V^{0+} as well as the split in the O-K edge. The HAADF-STEM micrograph in Figure S5 (Supporting Information) shows the unaltered microstructure of V_2O_5 before and after heat treatment. This structure was prepared on a TEM Protochip sample holder for in situ temperature-based TEM studies and was thermally cycled (three cycles) between 25 and 340 °C.

2.1. The Semiconductor-to-Metal Transition in Amorphous V_2O_5

The reduction of the refractive index *n* and the real dielectric constant ε_1 (Figure 2a; Figure S3, Supporting Information) upon exceeding the transition temperature can be attributed to a transition to a metallic – from an initial semiconducting state. At the same time, we do not observe plasmonic behavior with negative dielectric constants in the considered spectral range of 600 to 2100 nm (Figure 1), which is different from what was reported for VO_2 films.[41] Still, we assume that at longer wavelengths negative dielectric constants will be observed and an increase of the conductivity may be observed, as reported for VO_2.[38]

The major differences of the optical constants between 20 and 200 °C can be correlated with the initial changes facilitated probably by the evaporation of adsorbed surface adatoms/molecules, as shown in the first heating cycle of the resistivity measurement (Figure 3). Hence, the optical constants are reproducible and expected to follow a similar trend in the first cooling cycles as evidenced by in situ SIMS (**Figure 8**) and temperature-dependent resistivity measurements (Figure 3) for the subsequent three cycles. Furthermore, the variations in the optical constants are not very specific to the interface states as depicted previously by impedance spectroscopy of the high-frequency response.[27]

At the outset, the in situ temperature-dependent EELS measurements indicate a shift of the V-L_3 edge (Figure 7c) and the splitting of the O-K edges (Figure 7d) into two distinct peaks at 320 °C. This shows the formation of a strong metal–metal (V^{4+}–V^{4+}) interaction and a vanishing V^{5+}-contribution at temperatures above 320 °C. Based on in situ TEM studies[42] it is reported that upon annealing at 350 °C, O-K edges with two distinct peaks emerge along with the formation of nanocrystalline VO_2. However, in the present study, the split of the O-K edges disappeared, forming instead a single broad O-K edge centered at 532 and 531.8 eV for measurements done at 300 and 25 °C, respectively. It is important to note that, under a high vacuum environment and operating temperatures above 400 °C, the crystalline V_2O_5 structure shows decomposition and the associated formation of a reduced oxidation state.[43,44]

However, the present analysis shows that the V^{5+} state was regained and sustained upon cooling down to room temperature. The most plausible reason for this phenomenon seems to be a change of the van-der-Waals bond length, rather than considering it as induced by decomposition. In situ temperature-based X-ray diffraction studies, by Singh et al.[45] also reported a similar behavior: the absence of a decomposition process and a unique splitting of Bragg peaks of the V_2O_5 structure during heating to temperatures above 320 °C. The observed splitting of the XRD peaks was correlated with an elongation of the van-der-Waals bond.[45] This phenomenon is supported by dilatometric measurements on crystalline V_2O_5, where an unusually large coefficient of thermal expansion in the direction perpendicular to the van-der-Waals interaction layer was observed.[45,46] Additionally, the in situ electron diffraction study in the present work substantiated (Figures 5 and 6) no significant changes during thermal cycling between 25 and 340 °C. This observation clearly indicates

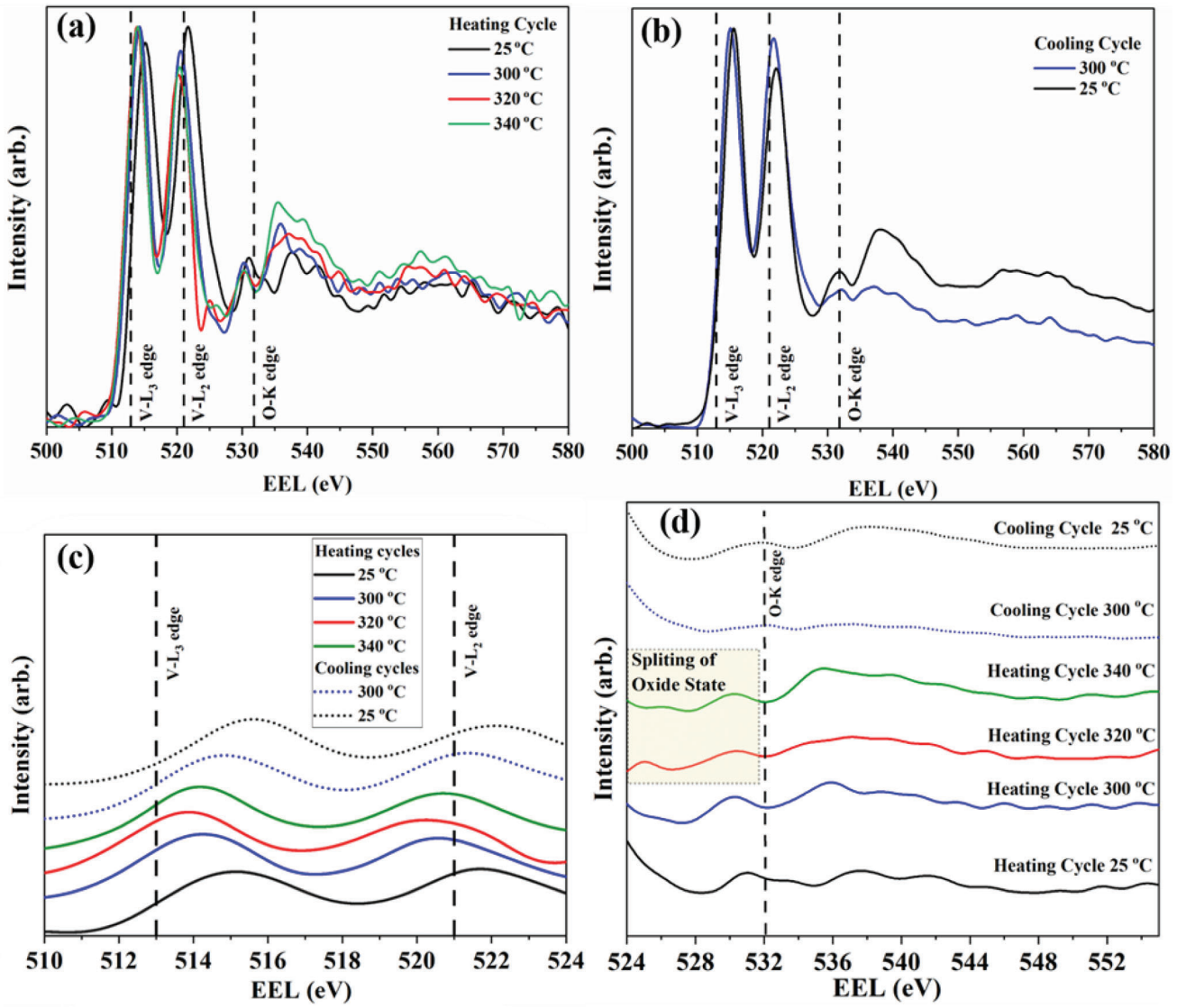

Figure 7. EEL Spectrum obtained during heating a), cooling b) cycles. Enlarged views c) of the shift of the edges of V-L_3 and V-L_2 and d) splitting of O-K edge at the SMT.

Table 1. Onset difference of O-K and V-L_3 edges as a function of temperature.

	Temperature [°C]	V-L_3 [eV]	V-L_2 [eV]	O K edge [eV]		ΔV-L_3 (with respect to V^{0+}) [eV]
				Edge 1	Edge 2	
Heating cycle	25	515.2	521.7	–	531	2.2
	300	514.3	520.6	–	530.3	1.3
	320	513.9	520.2	525	530.4	0.9
	340	514	520.4	526	530.3	1.0
Cooling cycle	300	515.1	521.7	–	532.0	2.1
	25	515.6	522.0	–	531.8	2.6

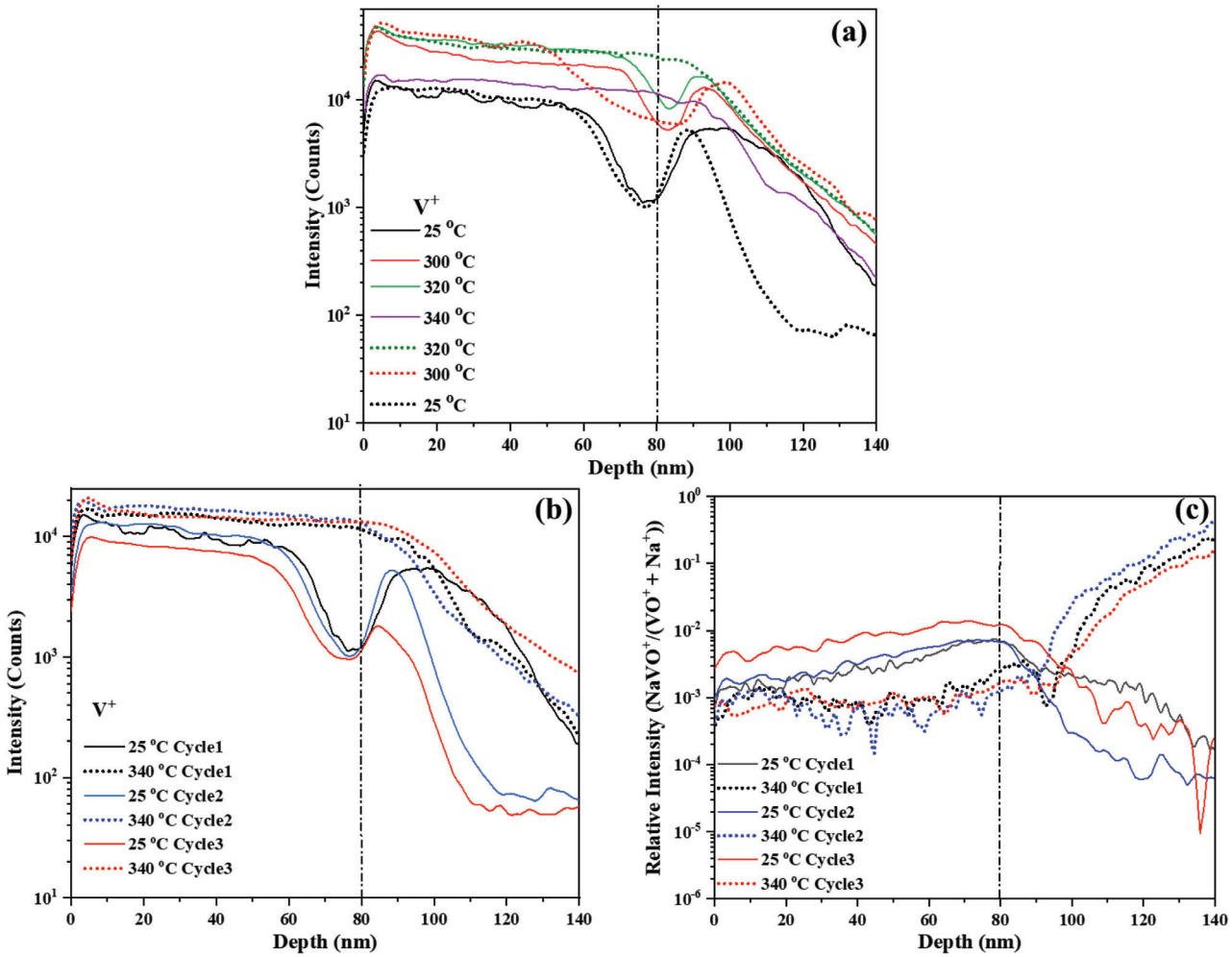

Figure 8. Elemental intensities obtained by ToF- SIMS as a function of temperature between 25 and 340 °C showing a) the variation in the intensity of V^+ in the first heating and cooling cycles, b) The comparison of the relative intensity variations measured during three subsequent heating and cooling cycles substantiating the reversible enhancement of the V^+ concentration (intensity) on both sides of the interface upon heating to 340 °C and its depletion while cooled to 25 °C. The relative intensity ratios of $NaVO^+$ /(VO^+ + Na^+) are shown in c) where the relative intensity ratio of $NaVO^+$ is seen to be enhanced in the substrate at high temperatures and is reversed to the initial state upon cooling.

the absence of a structural transformation that involves a disruptive change as involved in transitions that change the symmetry of a crystal lattice.

The Mott criterion describes that a phase transition in a material should satisfy the conditions: $a_B n_{cc}^{1/3} \approx 0.25$,[47,48] where a_B and n_{cc} are the effective Bohr radius and the charge carrier density, respectively. With respect to the Mott criterion, the metal-to-insulator transition in V_2O_5 is not expected to exist, due to its large value of "a_B".[44,47] However, the experimental data indicates that the van-der-Waals bond length might increase at a distinct temperature (i.e., the "transition" temperature).[49] Such an extension of the van-der-Waals bond length in V_2O_5 might cause a reduction of the "a_B". Within this picture, the reduction of a_B would further enhance the total "n_{cc}" by forming V^{4+}–V^{4+} interaction pairs, i.e. strengthening the contribution from a direct metal–metal interaction. a_B is directly proportional to the dielectric constant via the following relationship: $a_B = \hbar\varepsilon/(e^2 m^*)$ where m^* is the effective mass.[48,50] Such interpretation is in good agreement with the current experimental results, as indicated in Figure S3 (Supporting Information). The course of the dielectric function is in agreement with a (hypothetical) reduction of the "a_B". Further, the increase in metal-metal interaction is also substantiated by the shift of the V-L_3 edge to 513.9 eV at the SMT temperature, as depicted by the EELS spectra shown in Figure 7c.

The above interpretation also agrees with the most recent literature on the SMT of VO_2 and closes the existing gaps between observation and explanation. In several instances, the interaction of V^{4+}–V^{4+} (electron– electron) was found as a common factor of the SMT.[25,26,51,52] However, these earlier studies failed to explain the reason for its reversibility. In order to understand the possible metal-metal interactions in V_2O_5 and to understand the reversibility of the SMT, in situ SIMS analyses were performed. The detailed investigation of the interfacial reactions of the V_2O_5/glass thin film system is reported elsewhere.[27] Figure 8a shows the variation of the intensity of V^+ ions with increasing temperature. For better understanding, the V^+ ion intensity

at the lowest (25 °C) and at the highest (340 °C) temperatures are shown in Figure 8b. From the intensity plots of V^+ ions it is evident that a $NaVO^+$ interfacial layer is present, which was also demonstrated in.[27] The intensities of $NaVO^+$ and V^+ ions vary systematically in a reversible manner, both in the confined $NaVO^+$ interface layer and in VO^+ diffused soda-lime glass, as shown in Figure 8c. The variation of the relative intensities of V^+ ions is in strong correlation with the possibly increased charge carrier density derived from the EELS results presented in Figure 7. From the reversibility of the initial states, as indicated by the in situ SIMS measurements, the explanation by a possible structural phase transition can be ruled out for the SMT in V_2O_5. The reversibility of V^+ ion intensity, i.e. the regaining of the ionic state (V^{5+}) further strengthens the hypothesis that the increase in the van-der-Waals bond length that causes enhanced metal–metal interactions with increasing temperature is the reason for the SMT in amorphous V_2O_5.

Moreover, while correlating the reaction temperatures in DSC with SIMS data, it is obvious that the observed DSC signals fit the transition behavior of the thin film system. The obtained DSC results are in strong correlation with the available literature[3] on V_2O_5 gel exhibiting a prominent endothermic peak between 300 and 350 °C. The observed process was reversible and is reported to involve a significant modification of the coordination of V^{4+}. As mentioned earlier, the decomposition and the associated formation of a reduced oxidation state were reported to occur at temperatures above 400 °C in a high vacuum environment for crystalline V_2O_5,[43,44,53] therefore the current investigation has been limited to temperatures below 400 °C.

Even in the case of the well-studied VO_2, there is only one study mentioning structural changes according to a Mott-type phase transition.[22] However, many studies showed disagreement concerning such structural transformations for VO_2.[25,26,51,52,54] A recent report indicated the presence of both, an electronic state transition along with a structural Mott-type transition for VO_2.[52] Again, the observed reversibility of the transition along with the experimental data concerning the atomic as well as the electronic structures in dependence of temperature do not corroborate such interpretations for the present case. Instead, it should be emphasized that the data presented here can be fully rationalized by explaining the reversible SMT of V_2O_5 on the basis of a strong variation of the direct metal–metal interactions. These might not be limited to V^{4+}–V^{4+} interactions but might also be influenced by the V^+ – Metal interactions (from the substrate or external dopants, in the present study V–Na^+) that occur at the transition temperature. Furthermore, the present study suggests the potential extension of the investigation to other vanadium oxides, such as VO_2, known for phase transition behavior similar to V_2O_5. While V^{4+} has been more extensively studied than V^{5+}, exploring these interactions on amorphous states is challenging yet essential for a comprehensive understanding of these phenomena and goes beyond the scope of the present work.

As obtained from the EELS spectrum in Figure 7, the splitting of the O-K edge at the SMT was observed at ≈320 °C, which is in good agreement with the SMT revealed by other characterization techniques. These findings reveal that the SMT is caused by substrate-independent metal-metal interactions. Further, the in situ SIMS analyses indicate that the interfacial reactions impact the transition temperature.[27] Therefore, the choice of the semiconductor – or metal substrate along with the thin film processing techniques may influence the transition temperature without much impact on the transition behavior/mechanism.

The interface-induced metal-metal interactions at the transition temperature open up a new opportunity to tune the transition temperature and functionality of the V_2O_5 by engineering of incorporated metal ions (e.g., by varying the dopant concentration) for, e.g. thermo-electronic applications. The present results also motivate studying different vanadium oxides irrespective of their oxidation states or crystallinity, or vanadium-diffused or vanadium oxide-based semiconducting glasses under different atmospheric conditions.

3. Conclusion

The occurrence of a semiconductor-metal transition in V_2O_5 has been verified for a fully amorphous structure that remained amorphous throughout the transition. The optical constants showed a significant and reversible variation during heating and cooling the structure between room temperature and 340 °C. The amorphous structure of V_2O_5 was verified by both, in situ temperature-based electron diffraction and HAADF-STEM analyses before and after thermal cycling. The real-time observation of the SMT was proven via results obtained from EELS. At the SMT temperature of 320 °C, a reduced oxidation state of V is formed by a reversible splitting of the oxidation states. The origin of the SMT in amorphous V_2O_5 is explained by the V^{4+} interactions or metal-metal interactions. This explanation might be generalized to any form of V_2O_5. The current results indicate future prospects for tuning the phase transition temperature to fully utilize the SMT in advanced applications such as thermo-optical switches.

4. Experimental Section

Thin films of V_2O_5 were deposited on glass substrates (Thermo Fisher Scientific Silica-based microscope slides) using a vanadium metal target (99.95% purity) in a room-temperature reactive sputtering process. The DC Magnetron sputtering instrument (BesTech) was operated at a power of 40 W. The vacuum recipient was pre-evacuated to a pressure $< 7.5 \times 10^{-8}$ mbar and the working pressure was adjusted to 5×10^{-3} mbar with an O_2 to Ar ratio of (2:3) in terms of partial pressure. The thicknesses of the V_2O_5 thin films were determined to be approx. 80 nm using a surface profilometer (Bruker DektakXT) by averaging over a minimum of five measurements on at least two similarly processed samples. The sheet resistance (R_s) of the as-prepared V_2O_5 thin films on glass was measured at room temperature by a four-point probe setup (Keithley SCS – 4200). It is observed that the sheet resistance of amorphous V_2O_5 is in the semiconductor range (6.5×10^8 Ω per square) at room temperature.

The in situ temperature-based optical constants of the thin film were evaluated by spectroscopic ellipsometry (Semilab SE-2000), at an incidence angle of 70°, in the visible-to-NIR region (600–2100 nm).[55,56] A heating stage (Linkam Scientific Model TSEL1000V) operating under 2×10^{-5} mbar vacuum condition was used to heat/cool the structure between 20 and 340 °C with a rate of 10 °C min^{-1}. The dielectric functions of the bare glass substrate were measured and used to fit the optical constants of V_2O_5 using Semilab's SEA software. By considering an 80 nm V_2O_5 film thickness, the real and imaginary parts of the complex dielectric functions were extracted using the wavelength-by-wavelength method.[57] This method was generally used for lossy transparent materials (without a priori knowledge of material and dispersion relations), where the complex

dielectric functions were obtained directly from Ψ and Δ by extracting the real and imaginary parts numerically for each wavelength from the spectrum without the necessity to correlate with other wavelengths. The wavelength-by-wavelength extraction method was validated by performing the measurements at various angles between 50° and 70°, where it provides identical optical constants for each angle. Further, the optical constants were verified by measuring the optical properties of the V_2O_5 film and comparing with the calculated spectra using a transfer matrix method.

TEM was performed in a Thermo Fisher Scientific FEI Themis G3 60–300 operated at 300 kV. The microscope was employed to perform temperature-based EELS and to collect electron diffraction patterns. TEM and HAADF-STEM- modes were utilized for imaging the microstructure of V_2O_5, which was directly sputter-deposited on a copper grid as well as on a TEM Protochip sample holder (Fusion Heating FHBC series).

As the V_2O_5 thin film is electron and ion beam sensitive, the V_2O_5 thin film is directly sputter-deposited on the TEM Protochip sample holder (Fusion Heating FHBC series). A specialized mechanical masking-based method was developed for sample preparation, enabling precise alignment of the mask with specific areas on the TEM chip for the reactive sputter deposition of the V_2O_5 thin film. This approach ensures minimal damage to the samples, making them suitable for TEM analysis while avoiding the need for ion beam exposure in FIB-preparation. A thin film of stoichiometric V_2O_5, characterized by an amorphous phase and free from any defects or secondary vanadium oxide phases, has been successfully deposited using the method described in.[27] The detailed sample preparation method and the demonstration of its usage are presented elsewhere.[53]

EELS low-loss and high-loss spectra were obtained in the energy window of 0–200 eV and 500–700 eV, respectively. The temperature was controlled by the Protochip fusion software via a Keithley sourcemeter. Temperature profiles of 10 °C s^{-1} up to 300 °C and 1 °C s^{-1} for the temperature range of 300–340 °C were applied for both, heating and cooling cycles. Above 300 °C a low heating rate was applied to capture the minute changes in the diffraction pattern series. Further, a selective area electron diffraction pattern series was recorded at a rate of 1 frame per second with an aperture size of 40 µm. Spot EELS spectra were recorded at 25, 300, 320, and 340 °C during the heating cycle, and at 300 and 25 °C during the cooling cycle. In total 20 EELS spectra with an integration time of 4 ms (0.2 ms per frame) and 40 s (2 s per frame) were recorded for low-loss and high-loss spectral windows, respectively, with a dispersion of 0.1 eV. The power law background model was employed to fit the edges of V-L_3, V-L_2, and O-K. The V and O fundamental edges are identified with reference to the EELS Atlas digital library.[58]

Differential scanning calorimetry (DSC) was performed by a Diamond DSC (PerkinElmer). Heating and cooling cycles from 20 to 400 °C with a scanning rate of 100 °C min^{-1} were performed under Ar atmosphere at a pressure of 1.5 bar. In general, the magnitude of the DSC signal is proportional to the mass of the specimen which poses a major challenge when measuring thin films. For this reason, thin films with a higher thickness were used for DSC measurements to enhance the signal strength. It is to be noted that the transition temperature of amorphous V_2O_5 is not affected by the film thickness.

The depth profiles of the deposited thin films at the varying temperatures were measured using Time-of-Flight Secondary Ion Mass Spectroscopy (ToF-SIMS, IONTOF GmbH) with a custom-built device that is largely equivalent to the IONTOF M6. Standard samples of 1 cm × 1 cm were used to facilitate in situ measurements from the same single sample surface. For each measurement, sputtering is carried out over a 500 × 500 $µm^2$ area and the analyses were performed on data obtained over a 100 × 100 $µm^2$ region. The sample was held at the targeted temperature and sputtering was carried out while maintaining a constant temperature. The same procedure was followed for the measurements while heating and cooling. For each measurement, a new and fresh sputter area was selected on the sample surface. For a detailed description of the measurements and analysis of ToF-SIMS profiles, see ref. [27].

Supporting Information

Supporting Information is available from the Wiley Online Library or from the author.

Acknowledgements

A.C.M.E. and G.M.M. contributed equally to this work and the first co-authorship. G.M.M. and A.C.M.E. would like to thank the Alexander von Humboldt Foundation, Germany for the post-doctoral research fellowship. The authors also acknowledge Deutsche Forschungsgemeinschaft (DFG) for funding the TEM equipment via the Major Research Instrumentation Program under INST 211/719-1 FUGG. G.W. gratefully acknowledges partial funding by DFG. M.C., A.Y.P., and M.E. acknowledge financial support from the DFG (Project number 192346071 – SFB 986, subproject C1).

Open access funding enabled and organized by Projekt DEAL.

Conflict of Interest

The authors declare no conflict of interest.

Data Availability Statement

The data that support the findings of this study are available from the corresponding author upon reasonable request.

Keywords

electron energy-loss spectroscopy, ellipsometry, in situ transmission electron microscopy, in situ secondary Ion mass spectroscopy, phase transition, semiconductor to metal transition, vanadium oxide

Received: December 14, 2023
Revised: January 16, 2024
Published online: April 9, 2024

[1] E. P. Denton, H. Rawson, J. E. Stanworth, *Nature* **1954**, *173*, 1030.
[2] S. Narushima, H. Mizoguchi, K. Shimizu, K. Ueda, H. Ohta, M. Hirano, T. Kamiya, H. Hosono, *Adv. Mater.* **2003**, *15*, 1409.
[3] P. Aldebert, N. Baffier, N. Gharbi, J. Livage, *Mater. Res. Bull.* **1981**, *16*, 669.
[4] R.-P. Blum, H. Niehus, C. Hucho, R. Fortrie, M. V. Ganduglia-Pirovano, J. Sauer, S. Shaikhutdinov, H.-J. Freund, *Phys. Rev. Lett.* **2007**, *99*, 226103.
[5] M. Kang, I. Kim, S. W. Kim, J.-W. Ryu, H. Y. Park, *Appl. Phys. Lett.* **2011**, *98*, 131907.
[6] D. Porwal, A. C. M. Esther, I. N. Reddy, N. Sridhara, N. P. Yadav, D. Rangappa, P. Bera, C. Anandan, A. K. Sharma, A. Dey, *RSC Adv.* **2015**, *5*, 35737.
[7] A. Pergament, G. Stefanovich, V. Andreeev, *Appl. Phys. Lett.* **2013**, *102*, 176101.
[8] M. A. Hasan, A. K. Gupta, P. Bera, A. Dey, P. Y. Bhavanisankar, D. R. Kumar, S. Saha, N. Sridhara, A. Rajendra, S. Datta, *Ceram. Int.* **2022**, *48*, 35937.
[9] A. Dey, M. K. Nayak, A. C. M. Esther, M. S. Pradeepkumar, D. Porwal, A. K. Gupta, P. Bera, H. C. Barshilia, A. K. Mukhopadhyay, A. K. Pandey, K. Khan, M. Bhattacharya, D. R. Kumar, N. Sridhara, A. K. Sharma, *Sci. Rep.* **2016**, *6*, 36811.
[10] A. Dey, M. K. Nayak, M. S. Pradeepkumar, D. Porwal, B. Yougandar, A. Carmel Mary Esther, *Surf. Interface Anal.* **2017**, *49*, 805.

[11] D. Palai, A. Carmel Mary Esther, D. Porwal, M. S. Pradeepkumar, D. Raghavendra Kumar, P. Bera, N. Sridhara, A. Dey, *Philos. Mag. Lett.* **2016**, *96*, 440.
[12] J. Wang, Z. Zhang, R. Shi, B. N. Chandrashekar, N. Shen, H. Song, N. Wang, J. Chen, C. Cheng, *Adv. Mate. Inter.* **2020**, *7*, 1901582.
[13] H. Yin, K. Yu, C. Song, Z. Wang, Z. Zhu, *Nanoscale* **2014**, *6*, 11820.
[14] Y. Li, S. Ji, Y. Gao, H. Luo, P. Jin, *ACS Appl. Mater. Interfaces* **2013**, *5*, 6603.
[15] D. Mukherjee, A. Dey, A. C. Mary Esther, N. Sridhara, D. R. Kumar, A. Rajendra, A. K. Sharma, A. K. Mukhopadhyay, *RSC Adv.* **2018**, *8*, 30966.
[16] L. Hu, H. Tao, G. Chen, R. Pan, M. Wan, D. Xiong, X. Zhao, *J. Sol-Gel Sci. Technol.* **2016**, *77*, 85.
[17] N. Shen, S. Chen, Z. Chen, X. Liu, C. Cao, B. Dong, H. Luo, J. Liu, Y. Gao, *J. Mater. Chem. A* **2014**, *2*, 15087.
[18] W. Burkhardt, T. Christmann, S. Franke, W. Kriegseis, D. Meister, B. K. Meyer, W. Niessner, D. Schalch, A. Scharmann, *Thin Solid Films* **2002**, *402*, 226.
[19] Y. Lu, M. Stegmaier, P. Nukala, M. A. Giambra, S. Ferrari, A. Busacca, W. H. P. Pernice, R. Agarwal, *Nano Lett.* **2016**, *17*, 150.
[20] D. Q. Liu, W. W. Zheng, H. F. Cheng, H. T. Liu, *Adv. Mater. Res.* **2009**, *79–82*, 747.
[21] Z. Zhang, Y. Gao, H. Luo, L. Kang, Z. Chen, J. Du, M. Kanehira, Y. Zhang, Z. L. Wang, *Energy Environ. Sci.* **2011**, *4*, 4290.
[22] A. Moatti, R. Sachan, V. R. Cooper, J. Narayan, *Sci. Rep.* **2019**, *9*, 3009.
[23] M. Itoh, N. Akimoto, H. Yamada, M. Isobe, Y. Ueda, *J. Phys. Chem. Solids* **2001**, *62*, 351.
[24] A. Pergament, G. Stefanovich, *Phase Transitions* **2012**, *85*, 185.
[25] W.-T. Liu, J. Cao, W. Fan, Z. Hao, M. C. Martin, Y. R. Shen, J. Wu, F. Wang, *Nano Lett.* **2011**, *11*, 466.
[26] M. Yang, Y. Yang, B. Hong, L. Wang, K. Hu, Y. Dong, H. Xu, H. Huang, J. Zhao, H. Chen, L. Song, H. Ju, J. Zhu, J. Bao, X. Li, Y. Gu, T. Yang, X. Gao, Z. Luo, C. Gao, *Sci Rep* **2016**, *6*, 23119.
[27] C. M. E. Alphonse, M. M. Garlapati, B. J. Tyler, H. F. Arlinghaus, S. V. Divinski, G. Wilde, *Phys. Rapid Res. Ltrs.* **2021**, *15*, 2100077.
[28] K. Prajwal, A. Carmel Mary Esther, A. Dey, *Ceram. Int.* **2018**, *44*, 16088.
[29] A. C. M. Esther, A. Dey, D. Rangappa, A. K. Sharma, *Infrared Phys. Technol.* **2016**, *77*, 35.
[30] A. Sakunthala, M. V. Reddy, S. Selvasekarapandian, B. V. R. Chowdari, P. C. Selvin, *Energy Environ. Sci.* **2011**, *4*, 1712.
[31] Q. Lu, S. R. Bishop, D. Lee, S. Lee, H. Bluhm, H. L. Tuller, H. N. Lee, B. Yildiz, *Adv Funct Mater.* **2018**, *28*, 1803024.
[32] M. A. Hasan, S. Chavan, A. Dalal, A. Rajendra, A. Mondal, B. N. Sherikar, A. Dey, *Surf. Interface Anal.* **2021**, *53*, 844.
[33] N. Özer, *Thin Solid Films* **1997**, *305*, 80.
[34] A. Ashour, N. Z. El-Sayed, *J. Optoelectron. Adv. Mater.* **2009**, *11*, 251.
[35] A. C. M. Esther, D. Porwal, M. S. Pradeepkumar, D. Rangappa, A. K. Sharma, A. Dey, *Phys. B* **2015**, *478*, 161.
[36] S. Thiagarajan, M. Thaiyan, R. Ganesan, *New J. Chem.* **2015**, *39*, 9471.
[37] I. Muhammad, A. Ali, L. Zhou, W. Zhang, P. K. J. Wong, *J. Alloys Compd.* **2022**, *909*, 164797.
[38] R. T. Kivaisi, M. Samiji, *Sol. Energy Mater. Sol. Cells* **1999**, *57*, 141.
[39] H.-K. Kim, T.-Y. Seong, Y. S. Yoon, *J. Vac. Sci. Technol. B* **2003**, *21*, 754.
[40] D. S. Su, H. W. Zandbergen, P. C. Tiemeijer, G. Kothleitner, M. Hävecker, C. Hébert, A. Knop-Gericke, B. H. Freitag, F. Hofer, R. Schlögl, *Micron* **2003**, *34*, 235.
[41] J. B. Kana Kana, G. Vignaud, A. Gibaud, M. Maaza, *Opt. Mater.* **2016**, *54*, 165.
[42] B. Gauntt, E. Dickey, *Microsc. Microanal.* **2009**, *15*, 1002.
[43] R. J. D. Tilley, B. G. Hyde, *J. Phys. Chem. Solids* **1970**, *31*, 1613.
[44] D. S. Su, R. Schlögl, *Catal. Lett.* **2002**, *83*, 115.
[45] B. Singh, M. K. Gupta, S. K. Mishra, R. Mittal, P. U. Sastry, S. Rols, S. L. Chaplot, *Phys. Chem. Chem. Phys.* **2017**, *19*, 17967.
[46] I. Corvin, L. Cartz, *J. Am. Ceram. Soc.* **1965**, *48*, 328.
[47] A. L. Pergament, G. B. Stefanovich, A. A. Velichko, S. D. Khanin, *Condens. Matter. Leading Edge* **2006**, 1.
[48] N. F. Mott, L. Friedman, *Philos. Mag.* **1974**, *30*, 389.
[49] J. Chen, Z. Zhang, H. Lu, *Surf. Interfaces* **2022**, *33*, 102289.
[50] S. Beke, *Thin Solid Films* **2011**, *519*, 1761.
[51] S. Biermann, A. Poteryaev, A. I. Lichtenstein, A. Georges, *Phys. Rev. Lett.* **2005**, *94*, 026404.
[52] G. J. Paez, C. N. Singh, M. J. Wahila, K. E. Tirpak, N. F. Quackenbush, S. Sallis, H. Paik, Y. Liang, D. G. Schlom, T.-L. Lee, C. Schlueter, W.-C. Lee, L. F. J. Piper, *Phys. Rev. Lett.* **2020**, *124*, 196402.
[53] C. M. E. Alphonse, M. M. Garlapati, S. Hilke, G. Wilde, *Nano Select* **2020**, *1*, 413.
[54] H. T. Stinson, A. Sternbach, O. Najera, R. Jing, A. S. Mcleod, T. V. Slusar, A. Mueller, L. Anderegg, H. T. Kim, M. Rozenberg, D. N. Basov, *Nat. Commun.* **2018**, *9*, 3604.
[55] T. Krekeler, S. S. Rout, G. V. Krishnamurthy, M. Störmer, M. Arya, A. Ganguly, D. S. Sutherland, S. I. Bozhevolnyi, M. Ritter, K. Pedersen, A. Y. Petrov, M. Eich, M. Chirumamilla, *Adv. Opt. Mater.* **2021**, *9*, 2100323.
[56] M. Arya, A. Ganguly, G. V. Krishnamurthy, S. S. Rout, L. Gurevich, T. Krekeler, M. Ritter, K. Pedersen, M. Störmer, A. Yu Petrov, M. Eich, M. Chirumamilla, *Appl. Surf. Sci.* **2022**, *588*, 152927.
[57] H. Tompkins, E. A. Irene, *Handbook of Ellipsometry*, William Andrew, Norwich, NY **2005**.
[58] EELS Atlas, https://eels.info/atlas.